THE JOURNAL OF PHYSICAL CHEMISTRY Letters

Letter

pubs.acs.org/JPCL

Transient Absorption Spectroscopy of Excitons in an Individual Suspended Metallic Carbon Nanotube

Bo Gao,[†,‡] Gregory V. Hartland,[§] and Libai Huang*[,†]

[†]Radiation Laboratory and [§]Department of Chemistry and Biochemistry, University of Notre Dame, Notre Dame, Indiana 46556, United States

[‡]Department of Physics, Harbin Institute of Technology, Harbin, China

Supporting Information

ABSTRACT: We present femtosecond transient absorption measurements of individual metallic single-wall carbon nanotubes (SWNTs) to elucidate environmental effects on their spectroscopy and dynamics. Isolated suspended SWNTs were located using atomic force microscopy, and Raman spectroscopy was employed to determine the chiral index of select nanotubes. Transient absorption spectra of the SWNTs were obtained by recording transient absorption images at different probe wavelengths. This unique experimental approach removes sample heterogeneity in ultrafast measurements of these complex materials and provides a direct means to unravel the role of the substrate. The results show a ∼40 meV red shift of the lowest exciton transition, which is attributed to dielectric screening effects by the substrate. Energy relaxation in individual metallic nanotubes was observed with decay constants of a few hundred fs and about 10 ps. We attributed the fast and slow decay components to carrier scattering by optical and acoustic phonons, respectively.

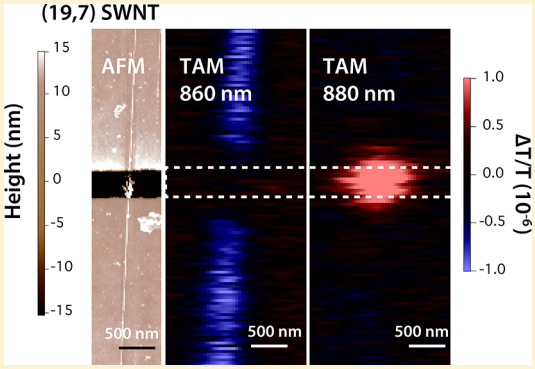

SECTION: Physical Processes in Nanomaterials and Nanostructures

Unlike bulk metals, where the formation of excitons is unlikely due to strong screening of the Coulomb interaction between electrons and holes by free carriers, excitons in metallic single-wall carbon nanotubes (SWNTs) have been predicted theoretically[1,2] and verified experimentally by Raman and Rayleigh scattering spectroscopy.[3] Exciton binding energies on the order of 100 meV have been observed, with excitonic transitions dominating the low-energy optical spectra.[3,4] However, many fundamental aspects of the properties of excitons in metallic SWNTs have not been explored in detail, such as intrinsic relaxation pathways and how the exciton properties are modulated by environment.

In part, this is because samples of SWNTs contain a large distribution of tube types, which makes it difficult to interpret the results of experiments. Size-selective separation techniques to enrich a single chirality have been developed almost exclusively for semiconducting SWNTs,[5,6] which makes studies of single chirality metallic SWNTs difficult. Single-particle measurements can circumvent this problem, and single-particle photoluminescence (PL) spectroscopy has been used to investigate excitons in semiconducting SWNTs.[7−11] However, PL studies of individual metallic SWNTs are not feasible because metallic SWNTs do not luminesce strongly. An alternative approach is to use absorption-based techniques to study single SWNTs.[12−14]

More recently, transient absorption (TA) spectroscopy has achieved single-nanostructure sensitivity[15−20] and has the advantage that it can provide dynamic as well as spectroscopic information. We have recently used TA measurements to record spectra of individual semiconducting SWNTs.[19] In this Letter, we elucidate exciton dynamics and spectra of individual suspended metallic SWNTs by single SWNT TA microscopy (TAM). In particular, we focus on the optical responses near the lowest excitonic resonance of metallic nanotubes. Our measurements provide a unique opportunity to unravel energy relaxation pathways of excitons in metallic SWNTs, as well as to reveal the role of the substrate in the spectroscopy and dynamics of these materials.

Highly oriented SWNTs with lengths of tens of micrometers were grown on single-crystal ST-cut quartz (Hoffman Materials Inc.) with $CoCl_2$ as the catalyst. The growth was performed in a tube furnace at 870 °C with a flow of methane (1000 sccm) and hydrogen (140 sccm) for 30 min. SWNTs were subsequently transferred onto a patterned glass coverslip with ∼400 nm wide and ∼250 nm deep trenches to obtain suspended tubes.[21] More details on sample preparation are presented in the Supporting Information (SI). By using a patterned substrate, the SWNTs can be precisely located so that Raman, atomic force microscopy (AFM), and TA spectroscopy can be performed on the same SWNT.[21] Raman spectra of individual SWNTs

Received: July 16, 2013
Accepted: August 27, 2013

   dx.doi.org/10.1021/jz401497n | J. Phys. Chem. Lett. 2013, 4, 3050−3055

were collected by a Renishaw Raman microscope (RM1000) with a 785 nm laser. Height images were collected with a Veeco Bioscope II AFM operating in tapping mode to confirm that the SWNTs were suspended.

Single SWNT TA measurements are based on the TAM setup described in our previous studies, and more details and a schematic of the setup are given in the SI.[19] Briefly, the tunable output (700−1000 nm) from a Ti:sapphire oscillator was split into two beams, one of which was employed as the probe and the other that was doubled by a β-barium borate (BBO) crystal to serve as the pump. The polarizations of the pump and probe beams were made parallel to the long axis of the SWNTs. The collinear pump and probe beams were focused at the sample with a 100×, 1.40 numerical aperture (NA) oil-immersion objective (Nikon). The transmitted beams were collected by a condenser (Nikon, NA 0.6), and the probe was detected with an avalanche photodiode (APD) (Hamamatsu C5331-04).

The pump−probe experiments measure the pump-induced differential change of the probe transmission, $\Delta T/T = (T_{\text{pump-on}} - T_{\text{pump-off}})/T_{\text{pump-off}}$. This was recorded by modulating the pump beam at 1 MHz with an acousto-optic modulator (Gooch & Housego) and monitoring the output of the APD with a lock-in amplifier (Zurich Instruments, HF2LI). Such high-speed modulation is necessary for achieving shot-noise-limited detection, which is needed for the small signal levels in these measurements. More detail on detection limit of the experiments is given in the SI.

TAM images were constructed by raster scanning the sample with a piezo stage and recording the relative change in transmittance ($\Delta T/T$) at fixed pump−probe delays. The ∼200 nm spot size of the pump and the ∼400 nm spot size of the probe at the sample implies that we can separate the response of two SWNTs if they are at least 200 nm apart. A pump fluence of 50 μJ/cm^2 at the sample was used for imaging. TA traces were obtained by recording the signal at a fixed spatial position and delaying the probe with respect to the pump with a mechanical translation stage (Newport Corp.). A pump fluence of 16 μJ/cm^2 (<1 exciton per 30 nm tube length) or lower was used for the dynamics measurements. For all measurements, the samples were placed under a continuous flow of argon gas to prevent damage. The time resolution at the sample was ∼400 fs for these experiments as determined from the fit to the rise of the TA signal.

Figure 1 shows tapping mode AFM height images of two SWNTs (SWNT-1 and SWNT-2) suspended over trenches, along with correlated TAM images at 0 ps. The AFM images of the suspended portions appear to be taller than they actually are due to problems with the AFM feedback mechanism when the tip is over the trench. The corresponding resonance Raman spectra of the supported portion of these two SWNTs recorded with 785 nm laser excitation are shown in Figure 2. The radial breathing mode (RBM) frequencies for the supporting parts of SWNT-1 and -2 are found to be 132.7 ± 0.3 and 130.5 ± 0.3 cm^{-1}, corresponding to diameters of 1.71 and 1.75 nm, respectively. We conclude that both SWNT-1 and -2 are metallic by using the Kataura plot for nanotube grown on a quartz substrate[22] when considering a RBM frequency of ∼130 cm^{-1} with an electronic resonance near 785 nm. From the Kataura plot, it can also be determined that the 785 nm excitation wavelength is close to the optical transition associated with the first subband E_{11}^{M}.

The TAM images in Figure 1 plot $\Delta T/T$ at 0 ps pump−probe delay. The dashed lines on the TAM images indicate the location of the trenches. The probe wavelengths are labeled on the images, and the pump wavelength is the second harmonic

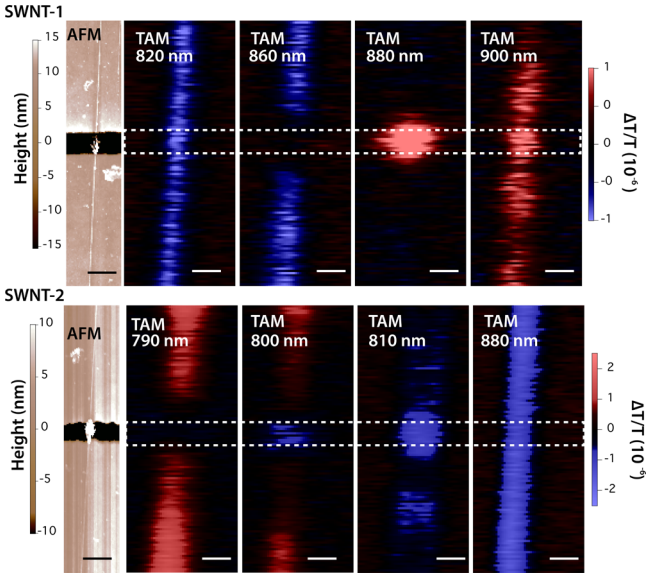

Figure 1. Correlated AFM height images (left) and TAM images of two SWNTs suspended over trenches. The probe wavelengths for the TAM images are labeled. The pump wavelength is the second harmonic of the probe. All TAM images were collected at a pump−probe delay of 0 ps. Dashed lines show the position of the trench. Scale bars are 500 nm in all images.

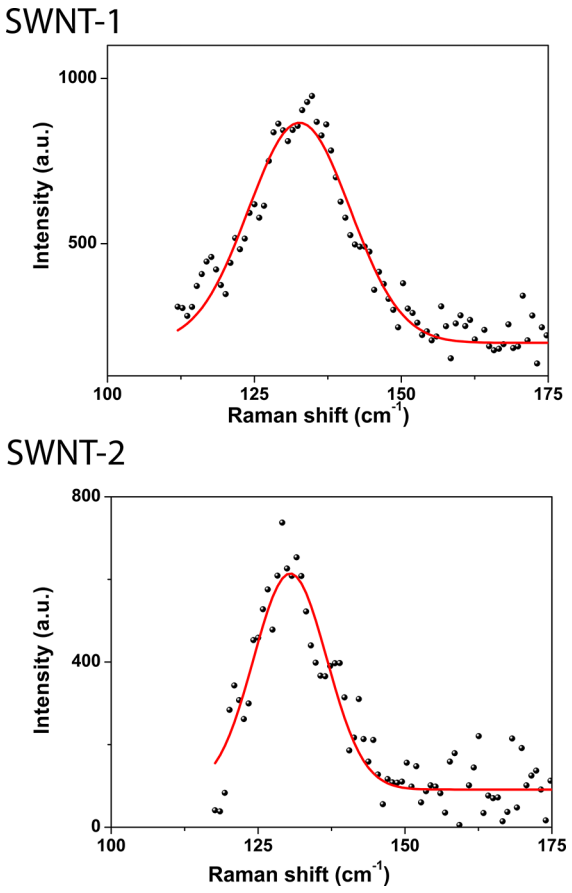

Figure 2. Resonance Raman spectra of SWNT-1 and SWNT-2 recorded with 785 nm laser excitation. The red solid lines are Gaussian fits of the experimental data.

dx.doi.org/10.1021/jz401497n | J. Phys. Chem. Lett. 2013, 4, 3050−3055

of the probe. In these experiments, the probe wavelength is scanned across the E_{11}^{M} transition, and the pump wavelength is close to but not in resonance with the E_{22}^{M} transition. Both SWNT-1 and SWNT-2 show wavelength-dependent $\Delta T/T$ signals. Two types of signals can be observed in a pump−probe experiment, namely, photoinduced bleach (PB) and photoinduced absorption (PA). The PB signal is in phase with the pump, corresponding to a positive $\Delta T/T$, while PA signal is out of phase with the pump, resulting in a negative $\Delta T/T$. Both ground-state bleaching and stimulated emission contribute to the PB signal, while excited-state absorption leads to the PA signal.

The TA signal of SWNT-1 changes from a PA (blue color in Figure 1) to a PB signal (red color in Figure 1) as the probe wavelength is tuned from 820 to 900 nm. In contrast, for SWNT-2, the signal changes from PB to a PA signal as the probe wavelength is tuned from 790 to 880 nm. Notable differences in TAM images are observed for the suspended and supported portions of the same nanotubes. For instance, at a probe wavelength of 800 nm, the suspended part of SWNT-2 displays a PA signal while the supported part shows a PB signal. For SWNT-1, the suspended part changes from PA to PB at a probe wavelength of 880 nm, while the supported part transitions at 900 nm.

Figure 3 plots the TA spectra at 0 ps ($\Delta T/T$ versus probe wavelength) for SWNT-1 and -2 to better illustrate the different responses from the supported and suspended parts of the nanotubes. The pump fluence was kept constant at 50 μJ/cm^2 for all wavelengths in these measurements. For SWNT-1, the PB for the SiO_2-supported part is red-shifted by ~25 nm (39 meV) compared to the suspended part. For SWNT-2, the PB band is not fully resolved due to the limited tunable range of the Ti:sapphire laser, but a similar trend is observed. Because bleaching occurs when the probe wavelength is resonant with the E_{11}^{M} transition, the shifts in the PB bands correspond to shifts in the E_{11}^{M} transition energies between the supported and suspended portions of the carbon nanotubes. Because the pump and probe wavelengths cannot be independently tuned, the recorded TA spectra could be distorted due to different absorption at different pump wavelengths. However, this distortion should be minimal because the pump wavelength is off-resonance and should not affect the conclusions drawn here.

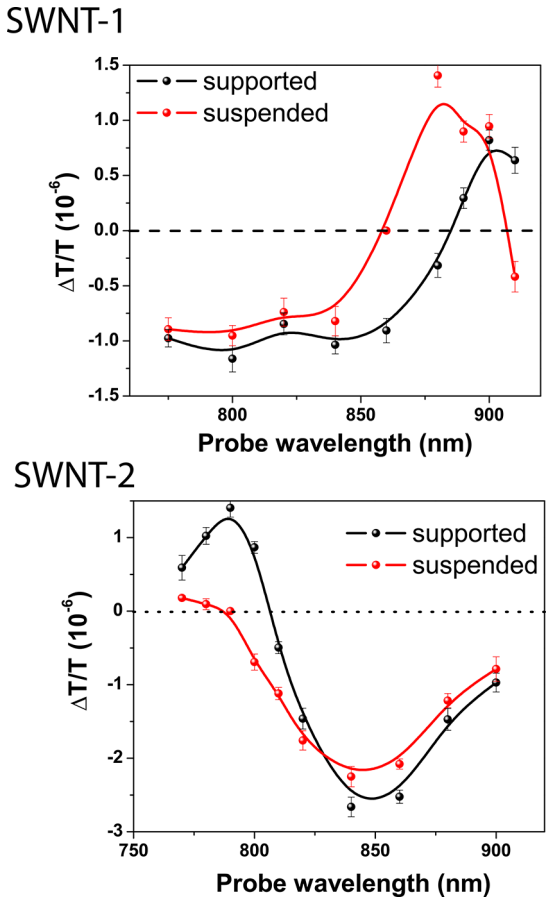

Figure 3. TA spectra at a 0 ps pump−probe delay time for SWNT-1 and -2. Suspended and substrate-supported portions of the nanotube are denoted by red and black spheres, respectively.

On the basis of the position of the PB band, we can refine the chirality assignment of the SWNTs. SWNT-1 has a RBM frequency of ~133 cm^{-1}. The five possible chiralities for this SWNT are (23, 2), (24, 0), (18, 9), (15, 12), and (19, 7), corresponding to E_{11}^{M} energies of 1.52, 1.53, 1.51, 1.47, and 1.43 eV, respectively.[23] In the TA spectra, the PB band of the suspended part of SWNT-1 is centered at ~870 nm or 1.43 eV. Therefore, we assign the chirality of SWNT-1 to be (19, 7). The PB band for the supported portion of SWNT-2 is close to 780 nm. Conclusive chirality assignment of SWNT-2 is not possible because the PB band is not fully resolved.

From Figure 2, it can be observed that the RBM line width for SWNT-1 (fwhm = 17 cm^{-1}) is much broader than that for SWNT-2 (fwhm = 12 cm^{-1}). This can be explained by the resonance condition of the Raman measurements. The RBM line width increases as the energy difference between E_{laser} and the resonant interband energy E_{ii} increases.[24] The E_{laser} used here is 785 nm, very much resonant with E_{11}^{M} for supported SWNT-2 with an observed PB band at 780 nm. In comparison, for supported SWNT-1 with an E_{11}^{M} at 900 nm, E_{laser} at 785 is much farther way from the resonance and leads to a much broader RBM line width.

For both nanotubes, PA bands are observed around the PB bands. Our previous study ascribed the origin of the PA bands to transitions from the single-exciton to biexciton energy levels.[19] PA bands red-shifted from the PB band were attributed to transitions from the lowest level in the E_{11} exciton manifold to levels in the $E_{11} + E_{ii}$ biexciton manifold.[19] Blue-shifted PA bands were assigned to the formation of a biexciton assisted by the G-mode optical phonons. We attributed the PA bands in the metallic SWNTs here to a similar origin.

The red shifts of PB bands for the SiO_2 substrate-supported portions of SWNTs are attributed to dielectric screening. Dielectric screening decreases both the electron−electron and electron−hole interactions in carbon nanotubes.[25] These interactions affect the optical transitions in different ways; electron−electron interactions cause a blue shift in the spectra through band gap renormalization, whereas electron−hole interactions lead to exciton formation and a red shift in the spectra.[26] The effects of dielectric screening have been extensively studied for semiconducting SWNTs. PL spectra from micelle-encapsulated SWNTs show average red shifts of 28 and 16 meV in E_{11}^{S} and E_{22}^{S}, respectively, compared to suspended semiconducting SWNTs.[27,28] Studies of SWNTs grown over trenches in various liquids with dielectric constants ranging from 1.9 to 37 showed red shifts in the PL spectra and PL excitation spectra of 30−50 meV for E_{11} and 20−30 meV for E_{22}, with the shifts saturating at ε = 5.[29] Resonant Raman

dx.doi.org/10.1021/jz401497n | J. Phys. Chem. Lett. 2013, 4, 3050−3055

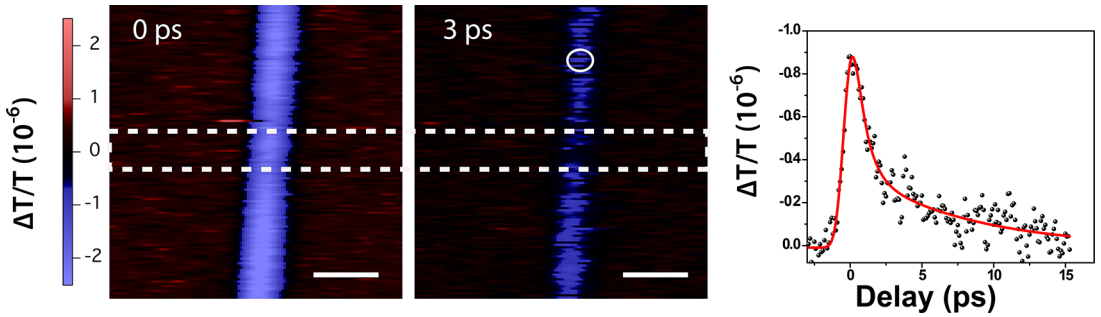

Figure 4. TA images of SWNT-2 at two different pump−probe delays of 0 and 3 ps with a probe wavelength of 840 nm and a pump wavelength of 420 nm. Dashed lines show the position of the trench. Scale bars are 500 nm in all images. The right panel shows a decay trace taken at the location as indicated by the circle in the middle panel. The red solid line is the fitting of the experimental data (black circles) with a Gaussian response function convoluted with a biexponential decay.

spectroscopy has also been used to probe the E_{22} energy in different dielectric environments and indicates a red shift of ∼30 meV in going from dry N_2 to water.[25] There is much less information available about dielectric screening effects in metallic SWNTs. Our measurements show a red shift of ∼40 meV for SWNT-1 supported by a glass substrate compared to that suspended over a trench, similar to what has been observed for semiconducting SWNTs. The small shifts observed for these systems are attributed to compensating changes in the band gap renormalization and exciton binding energies.[25]

Figure 4 depicts TAM images at two delay times of 0 and 3 ps, as well as a TA trace from SWNT-2. The trace was recorded at a location where the nanotube is supported by the substrate (indicated by the white circle in Figure 4). The data in Figure 4 were collected with a probe wavelength of 840 nm. This wavelength was chosen because it is near the PA band maximum for both the suspended and substrate-supported portions of SWNT-2. The trace was recorded with a pump fluence of 16 $\mu J/cm^2$, where exciton−exciton annihilation is expected to be negligible.[19] Dynamics taken near the PB band resonance at 790 nm for the supported portion of SWNT-2 are compared to dynamics taken at 840 nm in Figure S2 of the SI. Dynamics at the PB and PA bands are similar, indicating similar processes involved in the relaxation of both bands. Fitting the dynamics with a biexponential function convoluted with an instrumental response function yields decay constants of 760 ± 160 fs (63%) and 7.8 ± 1.1 ps (37%). Dynamics of SWNT-1 near the maximum of the PB band taken at a probe wavelength of 900 nm are illustrated in Figure S3 (SI). Fitting the dynamics of SWNT-1 results in decay constants of 350 ± 130 fs (54%) and 13.5 ± 1.1 ps (46%).

Direct measurement of the dynamics at suspended portions of the nanotubes was prevented by carbon deposition,[30,31] which occurs when the suspended nanotubes are irradiated for longer than 30 min (the time required to collect the dynamics data). Amorphous carbon deposits on both the suspended and supported portions of the carbon nanotubes but not on the bare substrate at the same laser power. Carbon deposition occurred more easily on suspended portions with lower laser power and shorter exposure time compared to supported portions. As a result, only qualitative comparison can be made between the energy relaxation for suspended and substrate-supported SWNTs. Comparing the TAM images at 0 and 3 ps in Figure 4 shows that there is no significant spatial heterogeneity in the dynamics induced by the substrate. Similar results were also observed for SWNT-1.

The dynamics observed in Figure 4 can be explained in the following way: interband excitation by ultrafast pulses first produces a nonequilibrium carrier distribution in the states that directly couple to the pump excitation. These hot (high-energy) carriers then thermalize through carrier−carrier scattering, resulting in electron and hole distributions over a broad energy range.[32] Carrier−carrier scattering is extremely fast in graphitic carbon, with a characteristic time of ∼10 fs,[33] which is beyond our temporal resolution of ∼400 fs. These carriers cool by interactions with optical and acoustic phonons. In carbon nanotubes and graphene, carrier−optical phonon scattering is the dominate cooling channel and occurs on a time scale of ∼200 fs.[19,34−38] Acoustic phonon scattering occurs at a slower time scale than optical phonon scattering, ranging from subpicoseconds to a few ps.[39]

Previous ensemble ultrafast measurements for metallic nanotubes have been complicated by the coexistence of semiconducting nanotubes as well as multiple chiralities in the ensemble.[40−42] This problem is circumvented here in our single-particle TA measurements. We attribute the ∼350 and ∼760 fs decay for SWNT-1 and SWNT-2, respectively, to optical phonon scattering. The 8 and 13 ps decay constants are ascribed to acoustic phonon scattering. Optical phonon scattering times of 350 and 760 fs are slower than the ∼200 fs time scale observed for graphene,[19,38] likely due the quantized nature of the phonon spectra in nanotubes.[43] The 8 and 13 ps acoustic phonon scattering time agrees well with theoretical predictions[39] and is similar to the ∼6 ps acoustic phonon relaxation time measured for (8,7) SWNTs.[44] The slower acoustic phonon scattering observed in our measurements maybe because of the larger diameter of SWNT-1 and SWNT-2 compared to that of the (8,7) SWNTs (1.75 and 1.71 nm compared to 0.9 nm). Acoustic phonon scattering is expected to be slower for large diameter tubes because of $1/d$ dependence of the carrier−phonon matrix element and the larger subband curvature that leads to less efficient acoustic phonon scattering.[39] A considerable difference in decay constants is observed for SWNT-1 and SWNT-2, and structure-dependent carrier−phonon scattering will be investigated in future studies.

In conclusion, femtosecond TAM was employed to study individual and suspended metallic SWNTs. TA spectra of SWNTs freely suspended and supported by the SiO_2 substrate were constructed by recording TA images at different probe wavelengths. The PB bands showed a ∼ 40 meV red shift for the substrate-supported compared to the suspended parts of the same nanotube, which is attributed to dielectric screening

dx.doi.org/10.1021/jz401497n | J. Phys. Chem. Lett. 2013, 4, 3050−3055

effects by the substrate. Energy relaxation in individual metallic nanotubes was also studied, and two decay constants were observed with time constants of a few hundred fs and ~10 ps. We attributed the fast and slow decay components to carrier scattering by optical and acoustic phonons, respectively.

■ ASSOCIATED CONTENT

Supporting Information

Details of the sample preparation, transient absorption miscroscopy experiments, the experimental setup, the shot-noise-limited detection experiments, and transient absorption traces from single SWNTs. This material is available free of charge via the Internet at http://pubs.acs.org.

■ AUTHOR INFORMATION

Corresponding Author

*E-mail: lhuang2@nd.edu.

Notes

The authors declare no competing financial interest.

■ ACKNOWLEDGMENTS

L.H. and B.G. acknowledge the support from the Office of Basic Energy Science of the U.S. Department of Energy (DE-FC02-04ER15533). G.V.H. acknowledges the support from the National Science Foundation through Award CHE-1110560. B.G. also acknowledges the National Science Foundation of China (No. 21203046) and new faculty start up funds from the Harbin Institute of Technology. This publication is contribution No. NDRL 4980 from the Notre Dame Radiation Laboratory.

■ REFERENCES

(1) Spataru, C.; Ismail-Beigi, S.; Benedict, L.; Louie, S. Excitonic Effects and Optical Spectra of Single-Walled Carbon Nanotubes. *Phys. Rev. Lett.* **2004**, *92*, 017403.

(2) Deslippe, J.; Spataru, C. D.; Prendergast, D.; Louie, S. G. Bound Excitons in Metallic Single-Walled Carbon Nanotubes. *Nano Lett.* **2007**, *7*, 1626−1630.

(3) Wang, F.; Cho, D. J.; Kessler, B.; Deslippe, J.; Schuck, P. J.; Louie, S. G.; Zettl, A.; Heinz, T. F.; Shen, Y. R. Observation of Excitons in One-Dimensional Metallic Single-Walled Carbon Nanotubes. *Phys. Rev. Lett.* **2007**, *99*, 227401.

(4) Doorn, S. K.; Araujo, P. T.; Hata, K.; Jorio, A. Excitons and Exciton−Phonon Coupling in Metallic Single-Walled Carbon Nanotubes: Resonance Raman Spectroscopy. *Phys. Rev. B* **2008**, *78*, 165408.

(5) Arnold, M. S.; Green, A. A.; Hulvat, J. F.; Stupp, S. I.; Hersam, M. C. Sorting Carbon Nanotubes by Electronic Structure Using Density Differentiation. *Nat. Nanotechnol.* **2006**, *1*, 60−65.

(6) Tu, X.; Manohar, S.; Jagota, A.; Zheng, M. DNA Sequence Motifs for Structure-Specific Recognition and Separation of Carbon Nanotubes. *Nature* **2009**, *460*, 250−253.

(7) O'Connell, M. J.; Bachilo, S. M.; Huffman, C. B.; Moore, V. C.; Strano, M. S.; Hároz, E. H.; Rialon, K. L.; Boul, P. J.; Noon, W. H.; Kittrell, C.; et al. Band Gap Fluorescence From Individual Single-Walled Carbon Nanotubes. *Science* **2002**, *297*, 593−596.

(8) Hartschuh, A.; Pedrosa, H. N.; Novotny, L.; Krauss, T. D. Simultaneous Fluorescence and Raman Scattering From Single Carbon Nanotubes. *Science* **2003**, *301*, 1354−1356.

(9) Wang, F.; Dukovic, G.; Brus, L. E.; Heinz, T. F. The Optical Resonances in Carbon Nanotubes Arise from Excitons. *Science* **2005**, *308*, 838−841.

(10) Htoon, H.; O'Connell, M.; Doorn, S.; Klimov, V. Single Carbon Nanotubes Probed by Photoluminescence Excitation Spectroscopy: The Role of Phonon-Assisted Transitions. *Phys. Rev. Lett.* **2005**, *94*, 127403.

(11) Hagen, A.; Steiner, M.; Raschke, M.; Lienau, C.; Hertel, T.; Qian, H.; Meixner, A.; Hartschuh, A. Exponential Decay Lifetimes of Excitons in Individual Single-Walled Carbon Nanotubes. *Phys. Rev. Lett.* **2005**, *95*, 197401.

(12) Berciaud, S.; Cognet, L.; Poulin, P.; Weisman, R. B.; Lounis, B. Absorption Spectroscopy of Individual Single-Walled Carbon Nanotubes. *Nano Lett.* **2007**, *7*, 1203−1207.

(13) Christofilos, D.; Blancon, J. C.; Arvanitidis, J.; Miguel, A. S.; Ayari, A.; Del Fatti, N.; Vallée, F. Optical Imaging and Absolute Absorption Cross Section Measurement of Individual Nano-Objects on Opaque Substrates: Single-Wall Carbon Nanotubes on Silicon. *J. Phys. Chem. Lett.* **2012**, *3*, 1176−1181.

(14) Oudjedi, L.; Parra-Vasquez, A. N. G.; Godin, A. G.; Cognet, L.; Lounis, B. Metrological Investigation of the (6,5) Carbon Nanotube Absorption Cross Section. *J. Phys. Chem. Lett.* **2013**, 1460−1464.

(15) Van Dijk, M. A.; Lippitz, M.; Orrit, M. Detection of Acoustic Oscillations of Single Gold Nanospheres by Time-Resolved Interferometry. *Phys. Rev. Lett.* **2005**, *95*, 267406.

(16) Mehl, B. P.; Kirschbrown, J. R.; House, R. L.; Papanikolas, J. M. The End Is Different Than the Middle: Spatially Dependent Dynamics in ZnO Rods Observed by Femtosecond Pump−Probe Microscopy. *J. Phys. Chem. Lett.* **2011**, *2*, 1777−1781.

(17) Lo, S. S.; Major, T. A.; Petchsang, N.; Huang, L.; Kuno, M. K.; Hartland, G. V. Charge Carrier Trapping and Acoustic Phonon Modes in Single CdTe Nanowires. *ACS Nano* **2012**, *6*, 5274−5282.

(18) Ruijgrok, P. V.; Zijlstra, P.; Tchebotareva, A. L.; Orrit, M. Damping of Acoustic Vibrations of Single Gold Nanoparticles Optically Trapped in Water. *Nano Lett.* **2012**, *12*, 1063−1069.

(19) Gao, B.; Hartland, G. V.; Huang, L. Transient Absorption Spectroscopy and Imaging of Individual Chirality-Assigned Single-Walled Carbon Nanotubes. *ACS Nano* **2012**, *6*, 5083−5090.

(20) Jung, Y.; Slipchenko, M. N.; Liu, C. H.; Ribbe, A. E.; Zhong, Z.; Yang, C.; Cheng, J.-X. Fast Detection of the Metallic State of Individual Single-Walled Carbon Nanotubes Using a Transient-Absorption Optical Microscope. *Phys. Rev. Lett.* **2010**, *105*, 217401.

(21) Jiao, L.; Xian, X.; Wu, Z.; Zhang, J.; Liu, Z. Selective Positioning and Integration of Individual Single-Walled Carbon Nanotubes. *Nano Lett.* **2009**, *9*, 205−209.

(22) Soares, J. S.; Cançado, L. G.; Barros, E. B.; Jorio, A. The Kataura Plot for Single Wall Carbon Nanotubes on Top of Crystalline Quartz. *Phys. Status Solidi B* **2010**, *247*, 2835−2837.

(23) Liu, K.; Deslippe, J.; Xiao, F.; Capaz, R. B.; Hong, X.; Aloni, S.; Zettl, A.; Wang, W.; Bai, X.; Louie, S. G.; et al. An Atlas of Carbon Nanotube Optical Transitions. *Nat. Nanotechnol.* **2012**, *7*, 325−329.

(24) Dresselhaus, M. S.; Dresselhaus, G.; Jorio, A.; Souza Filho, A. G.; Saito, R. Raman Spectroscopy on Isolated Single Wall Carbon Nanotubes. *Carbon* **2002**, *40*, 2043−2061.

(25) Walsh, A. G.; Vamivakas, A. N.; Yin, Y.; Cronin, S. B.; Unlu, M. S.; Goldberg, B. B.; Swan, A. K. Screening of Excitons in Single, Suspended Carbon Nanotubes. *Nano Lett.* **2007**, *7*, 1485−1488.

(26) Nugraha, A. R. T.; Saito, R.; Sato, K.; Araujo, P. T.; Jorio, A.; Dresselhaus, M. S. Dielectric Constant Model for Environmental Effects on the Exciton Energies of Single Wall Carbon Nanotubes. *Appl. Phys. Lett.* **2010**, *97*, 091905.

(27) Lefebvre, J.; Fraser, J. M.; Homma, Y.; Finnie, P. Photoluminescence From Single-Walled Carbon Nanotubes: A Comparison Between Suspended and Micelle-Encapsulated Nanotubes. *Appl. Phys. A: Mater. Sci. Process.* **2004**, *78*, 1107−1110.

(28) Bachilo, S.; Strano, M.; Kittrell, C.; Hauge, R.; Smalley, R.; Weisman, R. Structure-Assigned Optical Spectra of Single-Walled Carbon Nanotubes. *Science* **2002**, *298*, 2361−2366.

(29) Ohno, Y.; Iwasaki, S.; Murakami, Y.; Kishimoto, S.; Maruyama, S.; Mizutani, T. Excitonic Transition Energies in Single-Walled Carbon Nanotubes: Dependence on Environmental Dielectric Constant. *Phys. Status Solidi B* **2007**, *244*, 4002−4005.

(30) Bondi, S. N.; Lackey, W. J.; Johnson, R. W.; Wang, X.; Wang, Z. L. Laser Assisted Chemical Vapor Deposition Synthesis of Carbon Nanotubes and Their Characterization. *Carbon* **2006**, *44*, 1393−1403.

(31) Zhou, J.; Luo, Y.-S.; Li, L.-J.; Zhong, Q.-W.; Li, X.-H.; Yin, S.-P. Fabrication of Micro Carbon Pillar by Laser-Induced Chemical Vapor Deposition. *J. Cent. South Univ. Technol.* **2010**, *15*, 197−201.
(32) Ma, Y.-Z.; Hertel, T.; Vardeny, Z. V.; Fleming, G. R.; Valkunas, L. Ultrafast Spectroscopy of Carbon Nanotubes. *Top. Appl. Phys.* **2008**, *111*, 321−352.
(33) Breusing, M.; Ropers, C.; Elsaesser, T. Ultrafast Carrier Dynamics in Graphite. *Phys. Rev. Lett.* **2009**, *102*, 086809.
(34) George, P. A.; Strait, J.; Dawlaty, J.; Shivaraman, S.; Chandrashekhar, M.; Rana, F.; Spencer, M. G. Ultrafast Optical-Pump Terahertz-Probe Spectroscopy of the Carrier Relaxation and Recombination Dynamics in Epitaxial Graphene. *Nano Lett.* **2008**, *8*, 4248−4251.
(35) Sun, D.; Wu, Z.-K.; Divin, C.; Li, X.; Berger, C.; de Heer, W. A.; First, P. N.; Norris, T. B. Ultrafast Relaxation of Excited Dirac Fermions in Epitaxial Graphene Using Optical Differential Transmission Spectroscopy. *Phys. Rev. Lett.* **2008**, *101*, 157402.
(36) Newson, R. W.; Dean, J.; Schmidt, B.; van Driel, H. M. Ultrafast Carrier Kinetics in Exfoliated Graphene and Thin Graphite Films. *Opt. Express* **2009**, *17*, 2326−2333.
(37) Yan, H.; Song, D.; Mak, K. F.; Chatzakis, I.; Maultzsch, J.; Heinz, T. F. Time-Resolved Raman Spectroscopy of Optical Phonons in Graphite: Phonon Anharmonic Coupling and Anomalous Stiffening. *Phys. Rev. B* **2009**, *80*, 121403.
(38) Gao, B.; Hartland, G.; Fang, T.; Kelly, M.; Jena, D.; Xing, H. G.; Huang, L. Studies of Intrinsic Hot Phonon Dynamics in Suspended Graphene by Transient Absorption Microscopy. *Nano Lett.* **2011**, *11*, 3184−3189.
(39) Köhler, C.; Watermann, T.; Malic, E. Relaxation Dynamics via Acoustic Phonons in Carbon Nanotubes. *Phys. Status Solidi B* **2012**, *249*, 2483−2486.
(40) Ellingson, R.; Engtrakul, C.; Jones, M.; Samec, M.; Rumbles, G.; Nozik, A.; Heben, M. Ultrafast Photoresponse of Metallic and Semiconducting Single-Wall Carbon Nanotubes. *Phys. Rev. B* **2005**, *71*, 115444.
(41) Luer, L.; Lanzani, G.; Crochet, J.; Hertel, T.; Holt, J.; Vardeny, Z. V. Ultrafast Dynamics in Metallic and Semiconducting Carbon Nanotubes. *Phys. Rev. B* **2009**, *80*, 205411.
(42) Koyama, T.; Shimizu, S.; Saito, T.; Miyata, Y.; Shinohara, H.; Nakamura, A. Ultrafast Luminescence Kinetics of Metallic Single-Walled Carbon Nanotubes: Possible Evidence for Excitonic Luminescence. *Phys. Rev. B* **2012**, *85*, 045428.
(43) Hone, J.; Batlogg, B.; Benes, Z.; Johnson, A.; Fischer, J. Quantized Phonon Spectrum of Single-Wall Carbon Nanotubes. *Science* **2000**, *289*, 1730.
(44) Dyatlova, O. A.; Köhler, C.; Malic, E.; Gomis-Bresco, J.; Maultzsch, J.; Tsagan-Mandzhiev, A.; Watermann, T.; Knorr, A.; Woggon, U. Ultrafast Relaxation Dynamics via Acoustic Phonons in Carbon Nanotubes. *Nano Lett.* **2012**, *12*, 2249−2253.